Supplementary Information

Controllable approach to nitrogen defected ultrathin graphitic carbon nitride: Robust photo-redox properties and mechanism insights

Jun Hu, Hongyin Liu, Syed Aamir Hussain, Chenghui Hu, Feipeng Jiao*

School of Chemistry and Chemical Engineering, Central South University, Changsha 410083, People's Republic of China

***Corresponding author address:**

Prof. & Dr. Feipeng Jiao

School of Chemistry and Chemical Engineering, Central South University, Changsha 410083, China

E-mail: jiaofp@163.com

Text S1. Characterization

X-ray diffraction (XRD) was conducted on Bruker D8 Advanced instrument (Germany), equipped a Cu Kα radiation source (λ = 1.54 Å, 40 kV, 30 mA) at 10 °/min. X-ray photoelectron spectroscopy (XPS) was used on a Thermo Scientific ESCALAB Xi^+ instrument (Al Kα X-ray source) to study the chemical states of the materials. Scanning electron microscopy (SEM, TESCAN MIRA LMS) equipped with EDS and Transmission electron microscopy (TEM, FEI Tecnai F20, the Netherlands) were performed. Fourier transform infrared spectroscopy (FT-IR) was carried out on a Nicolet iS50FTIR instrument. N_2 adsorption-desorption isotherm and UV-vis DRS spectra were obtained on a Nova Station A (Quantachrome) and Shimadzu UV-2401 spectrophotometer (Germany), respectively. Photoluminescence (PL) analysis and Time-resolved PL decay curves (TRPL) were conducted on a Varian Cary Eclipse spectrometer. The electron spin resonance (EPR) was conducted on a Bruker EMXplus-6/1 (Germany). The electrochemical impedance spectroscopy (EIS), photocurrent response (TPR), and Mott-Schottky curves were carried out on an electrochemical workstation (CHI760E). The water contact angles were analyzed on an angle measuring instrument (JC 2000D1, Zhongchen Digital Equipment Co. Ltd., China). Solid-state ^{13}C magic angle spinning (MAS) NMR spectra were recorded on Burker AVANCE III HD 400 MHz WB solid-state NMR spectrometer at room temperature.

Text S2. Photocatalytic Hydrogen Evolution Test

The photocatalytic hydrogen evolution (PHE) experiments was measured on an online gas monitoring system on Labsolar-6A with a 300 W Xe lamp (BEIJING

Perfectlight Technology Co. Ltd., λ ≥ 400 nm). Specifically, photocatalysts (10 mg) was sonicated and dissolved in 100 mL (10 vol%) TEOA solution containing 3 wt% $H_2PtCl_6 \cdot 6H_2O$ as co-catalyst. The system temperature is controlled by circulating condensate at 5 °C. The photocatalytic system was further evacuated for 30 min and then 20 mL of argon was injected as a carrier gas to promote hydrogen circulation. After that, the photocatalytic test was performed. The content of hydrogen was examined by gas chromatography (GC9790II PLF-01). In addition, cyclic experiments were conducted by repeating the above experimental steps. The apparent quantum yield (AQY) was evaluated under the same conditions at monochromatic light. The formula is as follows.

$$\mathrm{AQY} = \frac{\text{Number of reacted electrons}}{\text{Number of incident light photons}} \times 100\ \%$$

Text S3. Photocatalytic Degradation Test

Photocatalytic degradation performance of the samples was measured by decomposing TC solution under visible light. Experimentally, 50 mg catalysts were dissolved ultrasonic into 50 mL of TC solution (20 ppm) and continuously stirred for 30 min under dark condition to achieve adsorption-desorption equilibrium. After that, the visible light is turn on and photocatalysis is going on. During the period of 30 min, 3.5 mL of reactive suspension was extracted and was collected by filtration with 0.45 μm filters. The absorption spectra of the supernatant were conducted on a UV-vis spectrophotometer (UV 9600) by measuring absorbance data at 357 nm. And then, changes in pollutant concentrations were measured according to Lambert-Beer law.

Text S4. DFT details

Density functional Theory (DFT) calculations were performed on the CASTEP module to construct N defect models. The generalized-gradient-approximation (GGA) of the Perdew–Burke–Ernzerhof (PBE) functional was utilized to study the exchange relationship calculation. Typically, the kinetic cutoff energy is 517.04 eV and k-point mesh is 2*2*1 for structure optimization. During the calculation process, the self-consistent field tolerance, maximum force, maximum displacement, and maximum stress are $1.0*10^{-6}$ eV, 0.03 eV $Å^{-1}$, 0.001 Å, and 0.05 GPa per atom, respectively. The band structure, Gibbs free energy, and potential density of states (PDOS) of pristine and N defected g-C_3N_4 were calculated after geometry optimization.

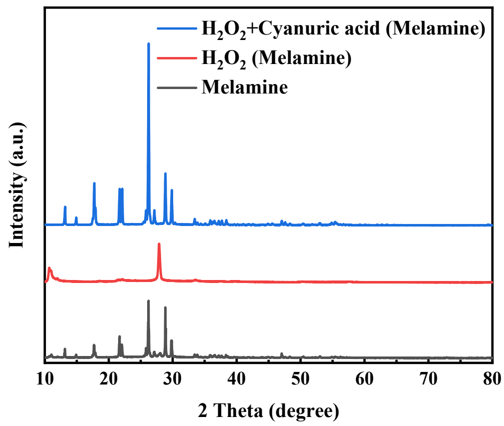

Figure S1. XRD patterns of melamine, H_2O_2-treated melamine, and H_2O_2-cyanuric acid-treated melamine.

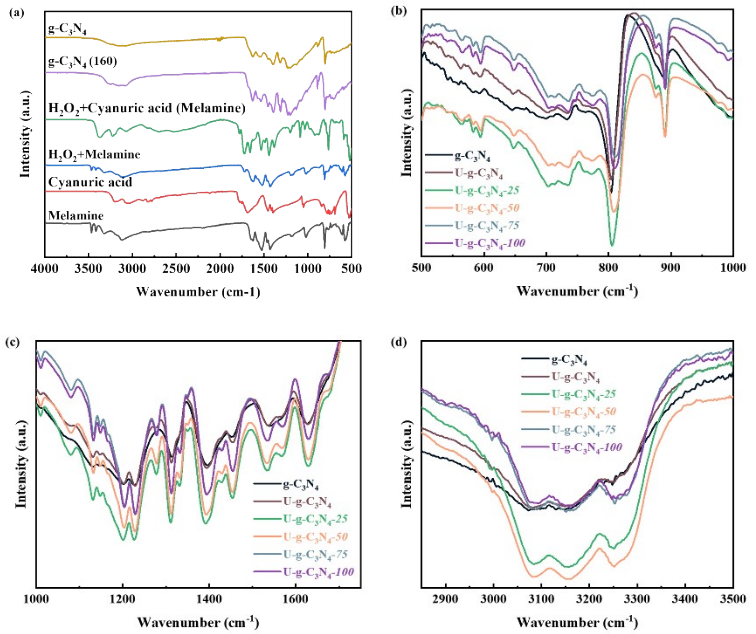

Figure S2. FT-IR spectra of (a) g-C_3N_4, g-C_3N_4 (160), melamine, cyanuric acid, H_2O_2-treated melamine, and H_2O_2-cyanuric acid-treated melamine. (b) 1000-500 cm^{-1}, (c) 1700-1000 cm^{-1}, and (d) 3500-2800 cm^{-1} FT-IR spectra of all samples.

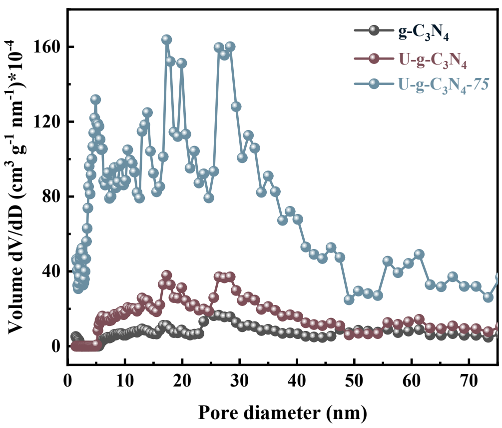

Figure S3. The pore size distribution curve of all samples.

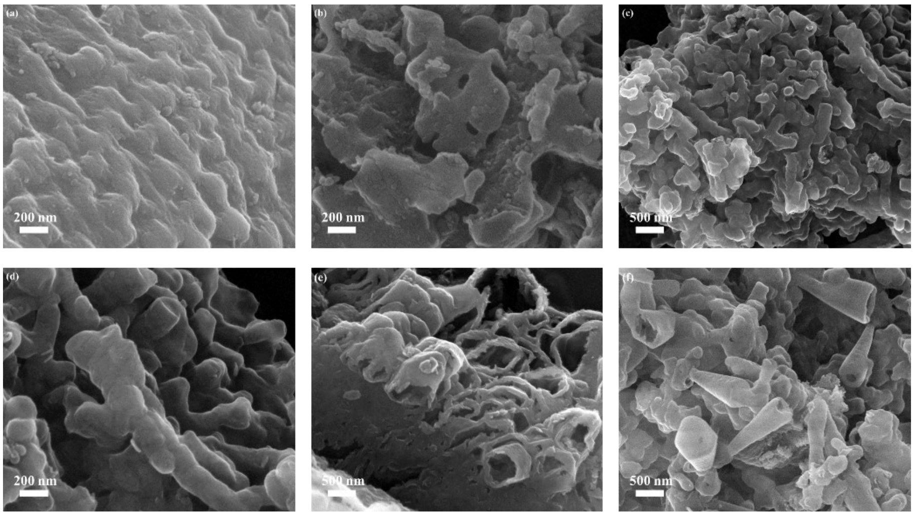

Figure S4. SEM images of (a) g-C_3N_4, (b) **U-g-C_3N_4**, (c) **U- g-C_3N_4-*25***, (d) **U- g-C_3N_4-*50***, (e) **U- g-C_3N_4-*75***, and (f) **U- g-C_3N_4-*100***.

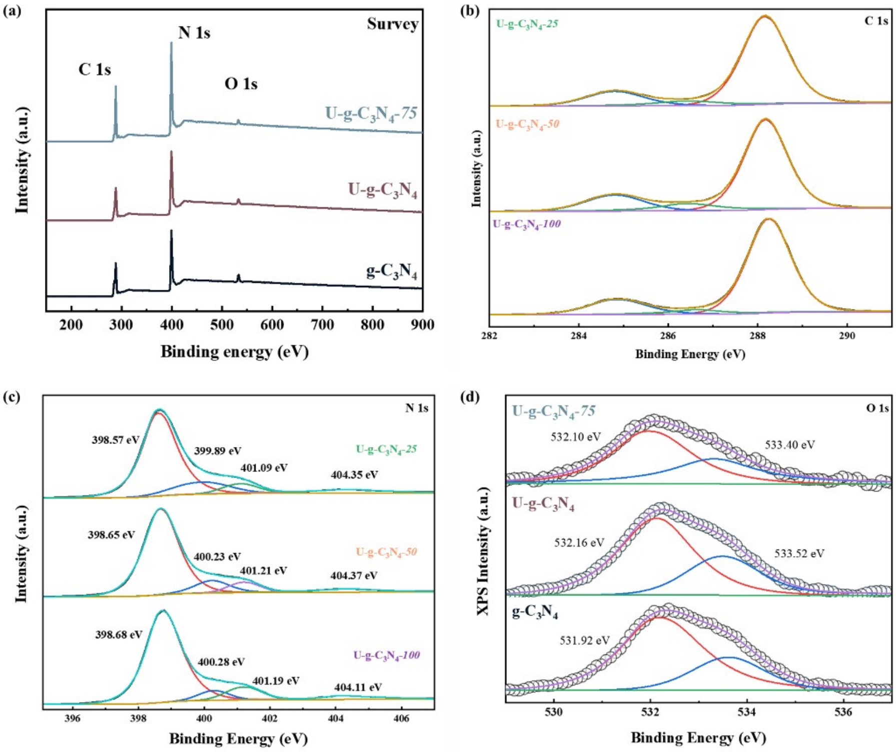

Figure S5. (a) XPS survey and (d) high-resolution O1s of g-C_3N_4, **U-g-C_3N_4**, and **U-g-C_3N_4-*75***. (b) high-resolution C1s and high-resolution N1s of **U-g-C_3N_4-*25***, **U-g-C_3N_4-*50***, and **U-g-C_3N_4-*100***.

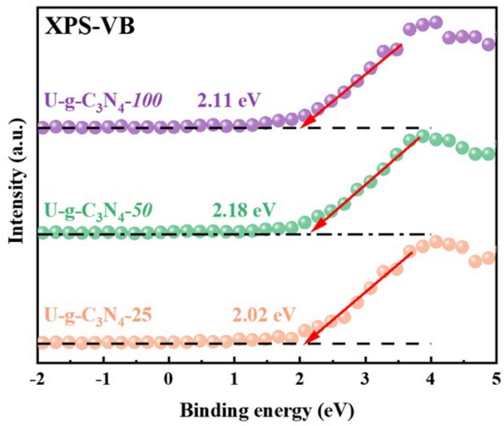

Figure S6. XPS-VB curve of **U-g-C_3N_4-*25*, U-g-C_3N_4-*50***, and **U-g-C_3N_4-*100***.

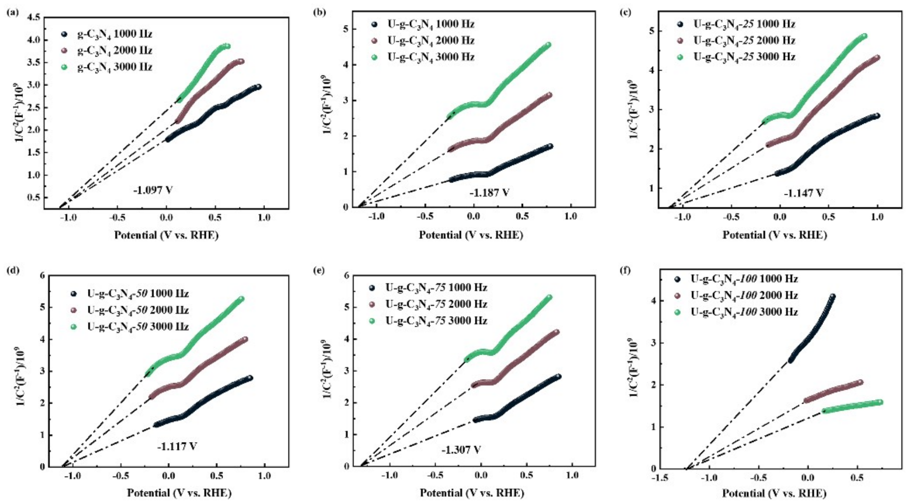

Figure S7. Mott-Schottky curves of g-C_3N_4, **U-g-C_3N_4, U-g-C_3N_4-*25*, U-g-C_3N_4-*50*, U-g-C_3N_4-*75*,** and **U-g-C_3N_4-*100***.

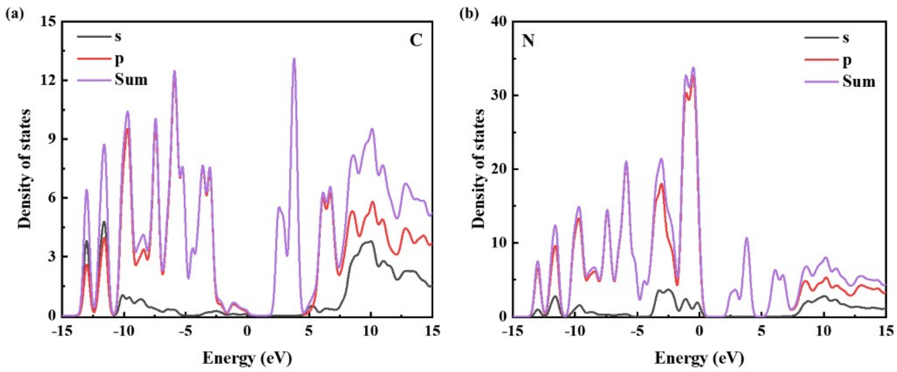

Figure S8. PDOS curves of (a) C and (b) N elements of g-C_3N_4.

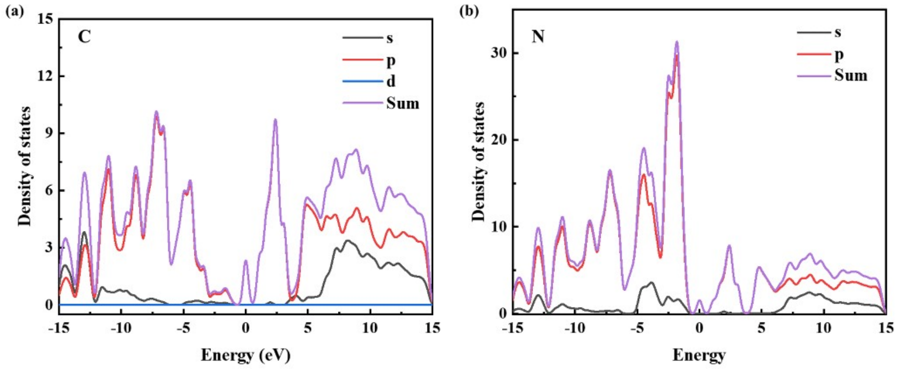

Figure S9. PDOS curves of (a) C and (b) N elements of **U-g-C_3N_4-*75***.

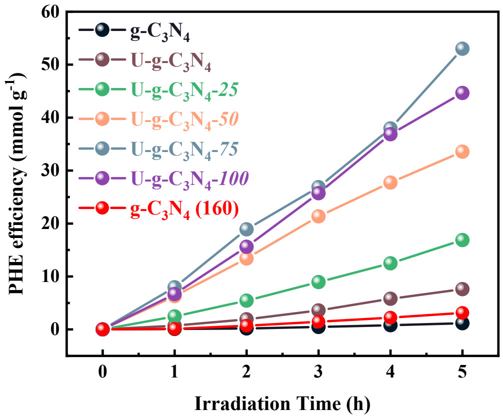

Figure S10. Photocatalytic H_2 production of **g-C_3N_4, U-g-C_3N_4**, and **U-g-C_3N_4-*n*** samples under full light spectra.

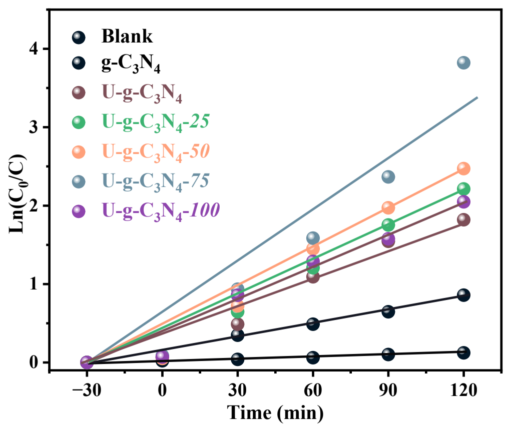

Figure S11. The first-order degradation kinetic fitting plot of the samples.

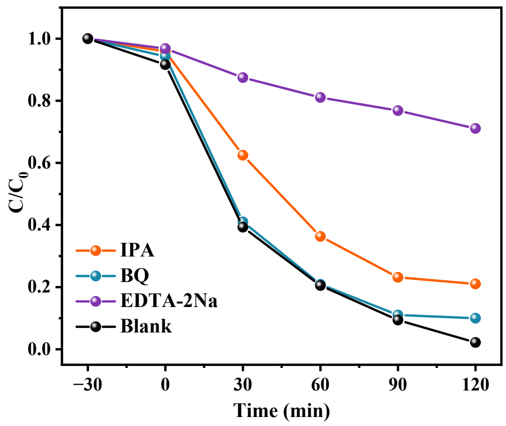

Figure S12. Trapping experiments of active species during TC degradation.

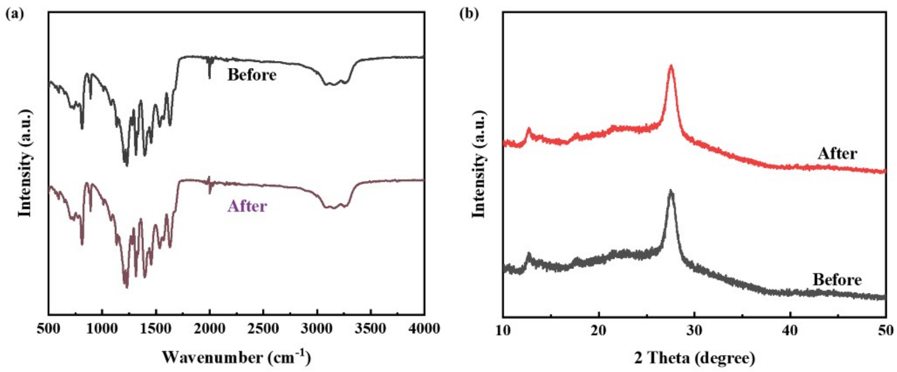

Figure S13. (a) FT-IR spectra and (b) XRD patterns of **U-g-C_3N_4-*75*** before and after used.

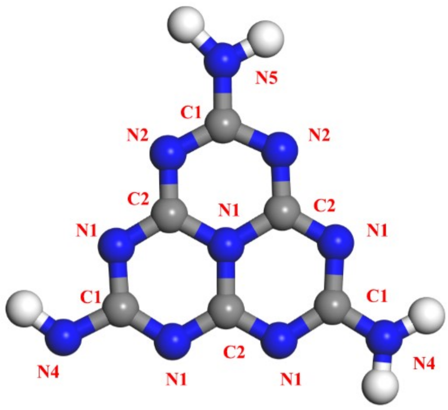

Figure S14. A typical melem unit with notations of carbon and nitrogen species.

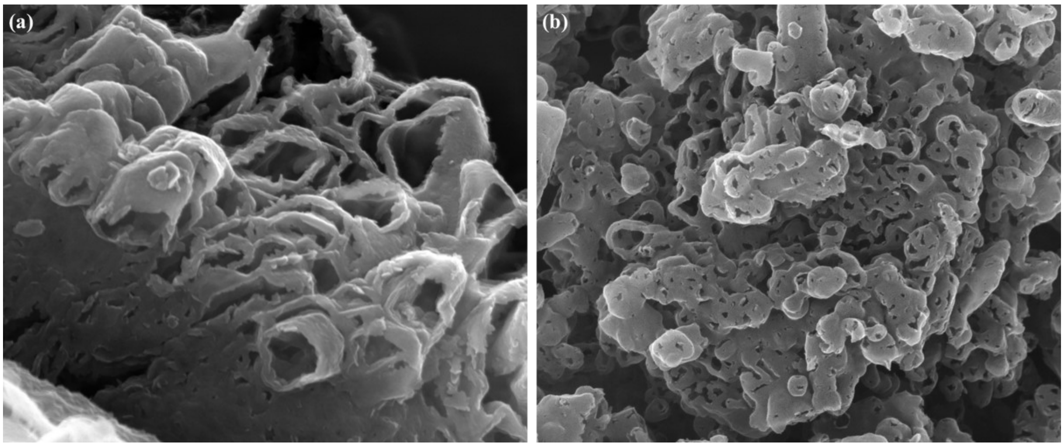

Figure S14. SEM images of samples before (a) and after (b) used.

Table S1. EDS data

	g-C_3N_4	**U-g-C_3N_4**	**U-g-C_3N_4-*25***	**U-g-C_3N_4-*50***	**U-g-C_3N_4-*75***	**U-g-C_3N_4-*100***
C	42.04	53.29	53.80	53.03	54.23	55.46
N	55.41	43.46	42.58	42.38	42.45	42.75
Ratios	0.75	1.22	1.26	1.25	1.27	1.29

Table S2. N-C=N/C-NH_x ratios of C1s XPS spectra of **g-C_3N_4, U-g-C_3N_4 and U-g-C_3N_4-*75*.**

group	**g-C_3N_4**	**U-g-C_3N_4**	**U-g-C_3N_4-*75***
N-C=N	35582	25179	18058
C-NH_x	11739	10479	5449
Ratios	7.53	9.92	22.29

Table S3. C=N-C/C3-N ratios of N1s XPS spectra of g-C_3N_4, **U-g-C_3N_4**, and **U-g-C_3N_4-75**.

group	**g-C_3N_4**	**U-g-C_3N_4**	**U-g-C_3N_4-75**
C=N-C	145810	190315	193858
C3-N	34328	20042	30269
Ratios	0.24	0.10	0.15

Table S4. C=N-C/C3-N ratios of N1s XPS spectra of **U-g-C_3N_4-25**, **U-g-C_3N_4-50**, and **U-g-C_3N_4-100**.

group	**U-g-C_3N_4-25**	**U-g-C_3N_4-50**	**U-g-C_3N_4-100**
C=N-C	195153	195747	217398
C3-N	40543	27235	18054
Ratios	0.20	0.13	0.08

Table S5. Comparison of PHE rate between **U-g-C_3N_4-*75*** and other different catalysts under visible light illumination.

Samples	Weight (mg)	Co-catalysts	Light-source	PHE rate(μmol/g/h)	References
U-g-C_3N_4-*75*	10	Pt (3 wt%)	300 W Xe Lamp	11072	This work
DCN-350	50	Pt (3 wt%)	300 W Xe Lamp	1542	[1]
D-TCN-450	25	Pt (1 wt%)	300 W Xe Lamp	789	[2]
PCNT-3	50	Pt (3 wt%)	300 W Xe Lamp	2020	[3]
CN-75	50	Pt (3 wt%)	300 W Xe Lamp	4158	[4]
Mo/S-g-C_3N_4-10	25	-	300 W Xe Lamp	290	[5]

C_3N_{4-x}-10	50	Pt (3 wt%)	300 W Xe Lamp	2460	[6]
U/AC-0.5	10	Pt (3 wt%)	300 W Xe Lamp	4470	[7]
CN-T125	100	Pt (3 wt%)	300 W Xe Lamp	905	[8]
Co-C_3N_4-C13/Pt	20	Pt (0.1 wt%) Co (0.2 wt%)	300 W Xe Lamp	2410	[9]
AV-g-C_3N_4	50	Pt (1 wt%)	300 W Xe Lamp	3700	[10]

Table S6. Comparison of photocatalytic degradation rate between **U-g-C_3N_4-*75*** and other different catalysts.

Samples	**Pollutants**	**Concentration (ppm)**	**Time (min)**	**Light-source**	**Degradation rate (%)**	**Reference s**
U-g-C_3N_4-*75*	TC	15	120	500 W Xe Lamp	97.8	This work
2D/3D-g-C_3N_4	TC	10	120	250 W Xe Lamp	69.6	[11]
g-C_3N_4-VNs	TC	10	120	300 W Xe Lamp	60.0	[12]
P-Mo-g-C_3N_4	TC	10	120	300 W Xe Lamp	69.0	[13]
Cyano-defects-g-C_3N_4	TC	10	60	300 W Xe Lamp	76.0	[14]
WO_3/g-C_3N_4/Bi_2O_3	TC	10	60	300 W Hg Lamp	80.2	[15]

WO_3/g-C_3N_4	TC	25	120	300 W Xe Lamp	70.0	[16]
Mo_2C/g-C_3N_4	TC	20	120	300 W Xe Lamp	76.0	[17]
Ag/O-K-g-C_3N_4	TC	20	60	300 W Xe Lamp	80.4	[18]

Reference:

[1] Y. Qin, J. Lu, X. Zhao, X. Lin, Y. Hao, P. Huo, M. Meng, Y. Yan, Nitrogen defect engineering and π-conjugation structure decorated g-C_3N_4 with highly enhanced visible-light photocatalytic hydrogen evolution and mechanism insight, Chem. Eng. J., 425 (2021) 131844.

[2] L. Chen, Y. Wang, S. Cheng, X. Zhao, J. Zhang, Z. Ao, C. Zhao, B. Li, S. Wang, S. Wang, H. Sun, Nitrogen defects/boron dopants engineered tubular carbon nitride for efficient tetracycline hydrochloride photodegradation and hydrogen evolution, Appl. Catal., B, 303 (2022) 120932.

[3] M. Wu, J. Zhang, B.-b. He, H. Wang, R. Wang, Y. Gong, In-situ construction of coral-like porous P-doped g-C_3N_4 tubes with hybrid 1D/2D architecture and high efficient photocatalytic hydrogen evolution, Appl. Catal., B, 241 (2019) 159-166.

[4] S. Zhao, J. Fang, Y. Wang, Y. Zhang, Y. Zhou, Poly(ionic liquid)-assisted synthesis of open-ended carbon nitride tube for efficient photocatalytic hydrogen evolution under visible-light irradiation, ACS Sustainable Chem. Eng., 7 (2019) 10095-10104.

[5] Y. Li, S. Zhu, Y. Liang, Z. Li, S. Wu, C. Chang, S. Luo, Z. Cui, One-step synthesis of Mo and S co-doped porous g-C_3N_4 nanosheets for efficient visible-light photocatalytic hydrogen evolution, Appl. Surf. Sci., 536 (2021) 147743.

[6] D. Wang, X. Gu, G. Liu, G. Huang, Y. Cao, Y. Guo, Employing one-step coupling cold plasma and thermal polymerization approach to construct nitrogen defect-rich carbon nitrides toward efficient visible-light-driven hydrogen generation, Int. J. Hydrogen Energy, 46 (2021) 5158-5168.

[7] X. Wang, Y. Zhao, H. Tan, H. Sun, Q. Shang, X. Zhao, T. Qiu, Y. Li, Foamer-derived bulk nitrogen defects and oxygen-doped porous carbon nitride with greatly extended visible-light response and efficient photocatalytic activity, ACS Appl. Mater. Interfaces, 13 (2021) 23866-23876.

[8] Q. Yang, W. Yang, F. He, K. Liu, H. Cao, H. Yan, One-step synthesis of nitrogen-defective graphitic carbon nitride for improving photocatalytic hydrogen evolution, J. Hazard. Mater., 410 (2021) 124594.

[9] Q. Zhang, X. Chen, Z. Yang, T. Yu, L. Liu, J. Ye, Precisely tailoring nitrogen

defects in carbon nitride for efficient photocatalytic overall water splitting, ACS Appl. Mater. Interfaces, 14 (2022) 3970-3979.

[10] J. Zhang, J. Chen, Y. Wan, H. Liu, W. Chen, G. Wang, R. Wang, Defect engineering in atomic-layered graphitic carbon nitride for greatly extended visible-light photocatalytic hydrogen evolution, ACS Appl. Mater. Interfaces, 12 (2020) 13805-13812.

[11] H. Dong, X. Zhang, J. Li, P. Zhou, S. Yu, N. Song, C. Liu, G. Che, C. Li, Construction of morphology-controlled nonmetal 2D/3D homojunction towards enhancing photocatalytic activity and mechanism insight, Appl. Catal., B, 263 (2020) 118270.

[12] H. Sun, F. Guo, J. Pan, W. Huang, K. Wang, W. Shi, One-pot thermal polymerization route to prepare N-deficient modified g-C_3N_4 for the degradation of tetracycline by the synergistic effect of photocatalysis and persulfate-based advanced oxidation process, Chem. Eng. J., 406 (2021) 126844.

[13] Y. Xu, Y. Liang, Z. Yuai, H. Long, Q. He, K. Guo, Y. Zhang, D. Chen, X. Xu, H. Hu, Co-doping g-C_3N_4 with P and Mo for efficient photocatalytic tetracycline degradation under visible light, Ceram. Int., 48 (2022) 24677-24686.

[14] Y. Lin, L. Wang, Y. Yu, X. Zhang, Y. Yang, W. Guo, R. Zhang, Y. Zhai, Y. Liu, Construction of molecularly doped and cyano defects co-modified graphitic carbon nitride for the efficient photocatalytic degradation of tetracycline hydrochloride, New J. Chem., 45 (2021) 18598-18608.

[15] L. Jiang, X. Yuan, G. Zeng, J. Liang, X. Chen, H. Yu, H. Wang, Z. Wu, J. Zhang, T. Xiong, In-situ synthesis of direct solid-state dual Z-scheme WO_3/g-C_3N_4/Bi_2O_3 photocatalyst for the degradation of refractory pollutant, Appl. Catal., B, 227 (2018) 376-385.

[16] T. Xiao, Z. Tang, Y. Yang, L. Tang, Y. Zhou, Z. Zou, In situ construction of hierarchical WO_3/g-C_3N_4 composite hollow microspheres as a Z-scheme photocatalyst for the degradation of antibiotics, Appl. Catal., B, 220 (2018) 417-428.

[17] Y. Wang, Z. Xing, H. Zhao, S. Song, M. Liu, Z. Li, W. Zhou, MoS_2@In_2S_3/Bi_2S_3 Core-shell dual Z-scheme tandem heterojunctions with broad-spectrum response and

enhanced photothermal-photocatalytic performance, Chem. Eng. J., 431 (2022) 133355.

[18] H. Lu, X. Li, F. Li, X. Xu, R. Zhao, C. Xiong, Q. Hu, Z. Miao, M. Tian, Construction of single-atom Ag embedded O, K co-doped g-C_3N_4 with enhanced photocatalytic efficiency for tetracycline degradation and Escherichia coli disinfection under visible light, J. Mol. Liq., 352 (2022) 118655.